Heat Transport Driven by the ITG and TEM Instabilities in the ASDEX-Upgrade Tokamak

F. Ryter[1], C. Angioni[1], M. G. Dunne[1], R. Fischer[1], B. Kurzan[1], A. Lebschy[1], R. M. McDermott[1], W. Suttrop[1], G. Tardini[1], E. Viezzer[2], and M. Willensdorfer[1]

The ASDEX-Upgrade Team

[1]*Max-Planck-Institut für Plasmaphysik, Garching, Germany*
[2]*Universidad de Sevilla, Seville, Spain*

Corresponding Author: F. Ryter, ryter@ipp.mpg.de

Turbulence-driven ion heat transport in tokamak H-modes is driven by the ion temperature gradient (ITG) instability, while electron heat transport is driven by the ITG, trapped electron mode (TEM) and/or electron temperature gradient (ETG) instabilities. These three instabilities appear above their respective threshold in normalized temperature gradient (R/LT) and drive transport. We present results on the role of these contributions to heat transport in the ASDEX Upgrade tokamak.

We performed dedicated experiments with neutral beam injection (NBI) which heats both electrons and ions and electron cyclotron resonant heating (ECRH) which heats the electrons. From modulating of the electron temperature with ECRH we deduce the electron heat pulse diffusivity (χ^{HP}) which reflects the stiffness directly and is complementary to the power balance diffusivity (χ^{PB}).

The predicted dependences of the ITG-driven ion heat transport on T_i/T_e and $E \times B$ rotational shear are found: the ITG is clearly more stable for high values of T_i/T_e and/or rotational shear. The ITG threshold itself could not be assessed experimentally with accuracy yet and experiments are foreseen in the near future to improve this situation.

The electron heat flux is partly driven by the ITG, but when increasing the electron heat flux with ECRH above the flux driven by the ITG, the TEM and/or ETG instabilities become unstable which is particularly visible in the modulation data. Indeed, a moderate increase of χ^{PB} and a stronger increase of χ^{HP} above $R/L_{T_e} = 5$ indicates unambiguously that an electron instability (TEM or ETG) develops above this threshold. The stiffness is close to that found in ASDEX-Upgrade for TEM-driven electron heat transport. Below the threshold, χ^{HP} and χ^{PB} exhibit about the same value of 1.5 m^2/s. This rather high value is attributed to the ITG-driven electron heat transport, in agreement with $\chi^{\mathrm{HP}} \approx \chi^{\mathrm{PB}}$ which reflects the fact that the ITG does not depend on ∇T_e. So far, we have found no indication of an ETG contribution predicted to exhibit a stronger stiffness.

Transport modelling and comparisons of the experimental results with gyrokinetic calculations will be presented for both the ITG and TEM/ETG studies.

Published as a journal article in Nuclear Fusion
http://iopscience.iop.org/article/10.1088/1741-4326/ab3061

HEAT TRANSPORT DRIVEN BY THE ITG AND ETG/TEM INSTABILITIES IN THE ASDEX UPGRADE TOKAMAK

F. RYTER, C. ANGIONI, M.DUNNE, R. FISCHER, B. KURZAN, A. LEBSCHY, R.M. MCDERMOTT, W. SUTTROP, G. TARDINI, M. WILLENSDORFER AND THE ASDEX UPGRADE TEAM[1]
Max-Planck-Institut für Plasmaphysik
Garching, Germany
e-mail of responsible author: ryter@ipp.mpg.de

E. VIEZZER
Dept. of Atomic, Molecular and Nuclear Physics,University of Seville
Seville, Spain

Abstract
A study of the properties of the turbulence-driven ion and electron heat fluxes, is presented. Dedicated H-mode experiments taking advantage of the on-axis and off-axis possibilities of both neutral beam injection and electron cyclotron resonance heating available on the ASDEX Upgrade tokamak were carried out. For the ion heat transport the threshold in normalized gradient above which the instability develops could be identified and its concomitant increase of the heat flux above it could be characterized in comparisons with non-linear gyro-kinetic calculations, yielding a good quantitative agreement. These results exhibit, as already known, a strongly stabilizing effect of the NBI fast ions when deposited in the central part of the plasma. The electron heat flux has been varied by adding electron cyclotron resonance heating demonstrating that above a certain level of applied electron heating, the ion temperature gradient instability does not suffice to drive the applied flux and that the electron temperature gradient instability develops to drive this additional flux. This result is assessed by gyro-kinetic calculations which in addition indicate that in these cases the trapped electron modes play a weak role.

1. INTRODUCTION

It is widely accepted that turbulence-driven ion heat transport in MHD quiescent tokamak H-modes is generally only driven by the ion temperature gradient (ITG) instability. But the ITG also drives a certain amount of electron heat flux, roughly proportional to the driven ion heat flux. In addition, contributions to the electron heat flux from trapped electron mode (TEM) and/or electron temperature gradient (ETG) instabilities are expected if the ITG is not sufficient to drive the electron heat flux imposed by the applied heating power. Kinetic ballooning modes do not contribute in the present study because the beta value is rather low ($\beta_N \leq 1.3$). According to theory, these three instabilities have the common property to appear above their respective threshold in normalized temperature gradient ($-R\nabla T/T = R/L_T$), T being the ion temperature (T_i) for the ITG and the electron temperature(T_e) for TEM and ETG. When R/L_T increases, the heat flux driven by each of these instabilities (q_i or q_e) increases above the corresponding threshold (R/L_{Tc}) with a slope which characterizes the so-called stiffness. A strong stiffness implies large variations of the heat flux for small variations in R/L_T such that the corresponding temperature profiles remain very close to the threshold. Conversely, in cases of weak stiffness larger excursions in R/L_T above R/L_{Tc} are expected.
In the present work we describe and discuss the experimental investigations carried out in the ASDEX Upgrade tokamak to assess the relative role of these different contributions to heat transport and determine the threshold and stiffness in comparisons with gyro-kinetic calculations.
For this purpose we performed dedicated H-mode experiments using the experimental possibilities available on the device, namely neutral beam injection (NBI) which heats both electrons and ions, as well as electron cyclotron resonant heating (ECRH) which heats exclusively the electrons. For both heating methods the power can be deposited centrally or off-axis, allowing us to vary the heat flux at a given radial position between the two depositions keeping the temperature variations moderate. The sum of the heating power outside of the off-axis deposition is kept almost constant such that the temperature almost does not vary. This is important because this implies that the boundary condition of the temperature profiles is constant. This is a now well established method to investigate heat transport, threshold and stiffness, as done in particular for the electron channel [1, 2, 3].
In addition, modulating the electron temperature with ECRH provides data for the so-called transient transport which yields directly the slope of the stiffness curve for electron heat transport, because of the dependence of q_e on ∇T_e [4, 5, 6]. From the modulation data the electron heat pulse diffusivity (χ_e^{HP}) is deduced, complementary to the power balance diffusivity (χ_e^{PB}), related by $\chi_e^{HP} = \chi_e^{PB} + \partial\chi_e/\partial(\nabla T_e)T_e$. If TEM and/or ETG modes contribute

[1] see A Kallenbach et al. Nuclear Fusion 57 (2017) 10201

to the electron heat transport above their threshold a variation of the electron heat flux and concomitantly of R/L_{Te} should reveal a strong increase of χ_e^{HP} at their threshold and χ_e^{HP} remains much larger than χ_e^{PB} if R/L_{Te} is further increased. This has been clearly demonstrated in AUG for TEM-dominated plasmas [1, 7] If the ITG instability only is the main drive of the electron heat flux, χ_e^{HP} remains low and very close to χ_e^{PB}, because q_e driven by the ITG depends very weakly on ∇T_e, as shown for AUG in [7].
The experiments described in the present paper are based on these properties. The experimental data are provided by the usual diagnostics, in particular the 60 channel ECE radiometer complemented by the Thomson scattering for T_e and the CXRS measurements for T_i and rotation. The heating power deposition calculations and power balance analyses are performed with the TRANSP code [8]. Two distinct series of H-mode experiments with similar parameters were carried out to investigate the ion and electron channels respectively, as described below.

2. ION HEAT CHANNEL

2.1. EXPERIMENTAL RESULTS

The stability of the ITG depends on several plasma quantities: T_e/T_i, β, radial shear of the toroidal rotation, ion dilution by impurities or fast ions, stabilization by fast ions. These dependences affect the stiffness and/or the threshold of the instability as follows:
- T_e/T_i is destabilizing such that the stiffness increases and the threshold decreases when T_e/T_i increases, [9, 10]. The threshold also increases with normalized shear $\hat{s}/q$, [11].
- High shear of the toroidal rotation is stabilizing and increases the threshold [12];
- NBI fast ion effects reduce the stiffness and increase the threshold trough ion dilution [13] and non-linear effects, in particular at high β, [14, 15].
In our experiments to the ITG-driven ion heat flux, we performed H-mode plasmas in the usual range of ASDEX Upgrade: $P_{NBI} \approx 5MW$, plasma current of 0.8 MA at a magnetic field of 2.6 T, yielding $q_{95} \approx 5$, at a line averaged density of about 6 $10^{19}\mathrm{m}^{-3}$, corresponding to a Greenwald fraction of about 0.55. These deuterium plasmas were quite pure with $Z_{eff} \approx 1.1$. The aim was to vary the ion heat flux in the central region by applying either on-axis or off-axis NBI. In addition ECRH power was also deposited in the plasma center, at three different levels: 0.65, 1.5 and 2.75 MW. The lowest power was used to avoid tungsten accumulation during the NBI off-axis phases, the higher levels to vary T_e/T_i and study its impact on the ITG. The case with $P_{ECRH} = 0.65$ MW is illustrated in figure 1. The left plot shows that, in the off-axis case, the ion heat power deposition is low inside of $\rho_{tor} \leq 0.4$. This is

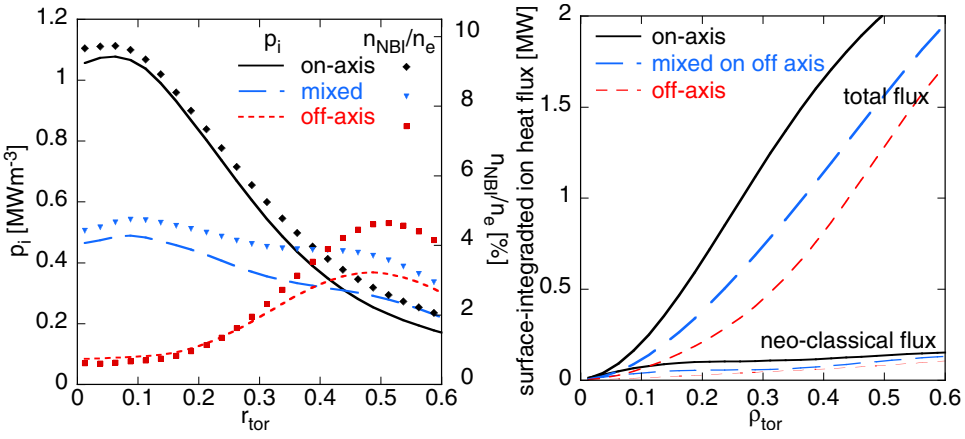

FIG. 1. Ion heating for on-axis, off-axis and mixed NBI deposition in the central region ($\rho_{tor} \leq 0.6$), for the case $P_{ECRH} = 0.65$ MW. Left panel: ion heat deposition profiles. Right panel: surface-integrated ion heat flux.

therefore where the analysis must be carried to have a large variation in ion heat flux including a low value in the purely off-axis case to approach the ITG threshold in R/L_{Ti}. The corresponding variation of the surface-integrated ion heat flux (Q_i) is shown in the right plot, indicating that a variation of Q_i of about a factor of three could be achieved in the inner region. We also plotted the heat flux driven by neo-classical transport which is much smaller than that the total flux, showing that turbulent transport dominates. In the following we labelled turbulent transport the quantity $Q_{i,turb} = Q_i - Q_{NC}$.
Figure 2 shows the corresponding variations of the T_e and T_i profiles. These are rather small for T_e, mainly due to the fact that ECRH (0.65 MW) was deposited in the center and causes $T_e > T_i$. For the higher ECRH levels,

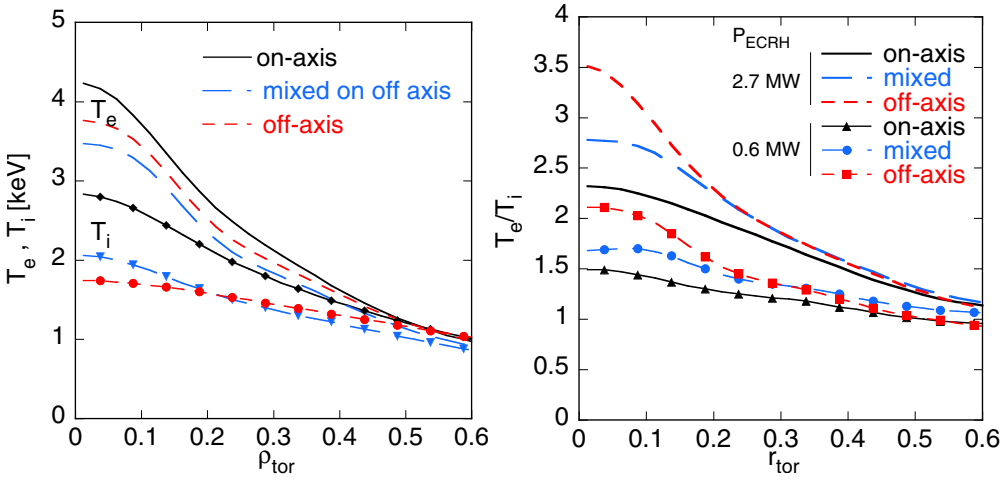

FIG. 2. T_e and T_i profiles for on-axis, off-axis and mixed NBI deposition in the central region, $\rho_{tor} \leq 0.6$, fits used for the TRANSP calculations. For clarity the experimental data points are not shown. The dots on the T_i profiles are not measured data but only for easier identification of the profiles.

T_e is much higher and varies even less (not shown). In contrast, ∇T_i varies by about a factor of 2 in the region $0.20 \geq \rho_{tor} \geq 0.40$ where the largest variation in the ion heat flux occurs. Note that for the off-axis case (low Q_i), the T_i profile is very flat. The T_i values in this radial region vary much less than the gradient, as shown quantitatively below. Further, it is worth underlying that, as pointed out above, T_i at $\rho_{tor} \geq 0.5$ is almost constant independently of the heat scheme which is expected as the ion heat flux varies little in the outer part of the plasma. This is important because the value of T_i at mid radius is the boundary condition for the T_i profiles inside this region such that those are solely determined by transport and heat flux and not by an external condition, e.g. pedestal top. This indicates that the experiments worked as expected. Not shown here are the profiles of the toroidal plasma rotation which are very flat in the off-axis case but rather peaked in the on-axis case.

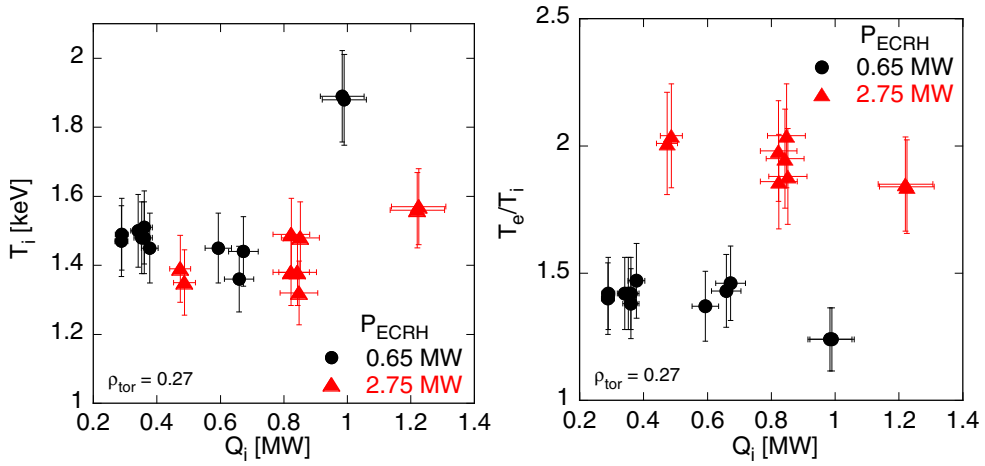

FIG. 3. Left panel, variation of T_i versus ion heat flux in the NBI on-axis off-axis experiments for the two cases with low and high ECRH power, 0.65 and 2.75 MW respectively. Right plot, corresponding values of T_e/T_i.

We made the analysis of the dependence of the ion heat flux upon R/L_{Ti} at $\rho_{tor} \approx 0.27$. The results for the two cases with P_{ECRH} 0.65 MW and 2.75 MW are shown in the next figures. Figure 3 left panel illustrates the behaviour of T_i for the two cases: as already indicated above, the overall variation is small, less than 20%, the largest change corresponds to the on-axis NBI case with the highest Q_i value, for which T_i is clearly higher than the other two cases. We will come back to this when discussing the gyrokinetic calculations. Figure 3 right panel indicates that, as expected, T_e/T_i is clearly larger for the P_{ECRH} = 2.75 MW case, but the variation of T_e/T_i with Q_i is small for each of the cases. This is important for the analysis as the impact of T_e/T_i on the ITG stability remains

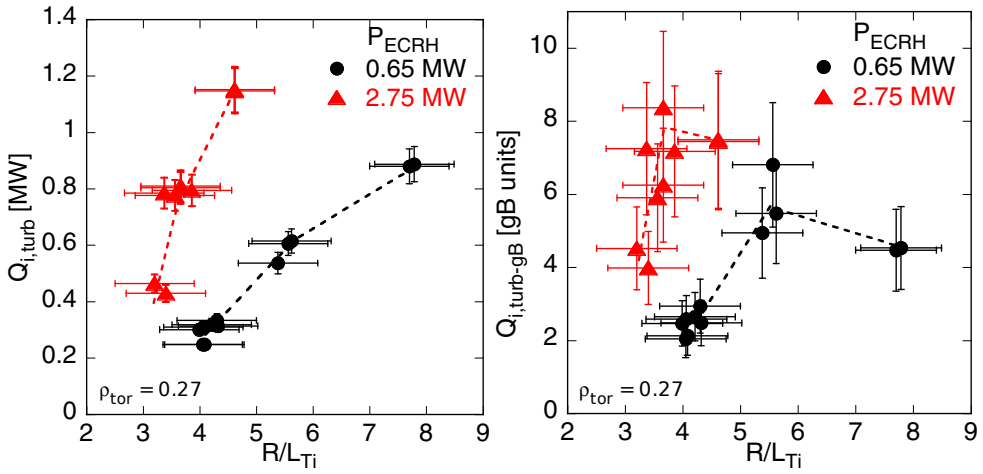

FIG. 4. Ion heat flux versus R/L_{Ti} experimental results for the variation of on-axis and off-axis NBI deposition. Left plot surface-integrated ion heat flux, right plot ion heat flux normalized by the gyro-Bohm assumption. The lines are only to guide the eye.

weak for each of the P_{ECRH} cases.

The relation between ion flux and R/L_{Ti} is shown in figure 4 left panel for the surface-integrated turbulent flux. It reveals in both cases a clear increase of the heat flux with R/L_{Ti}. This is in agreement with the hypothesis that the ITG is destabilized above a threshold and that the ITG-driven flux increases with R/L_{Ti} above this threshold. It exhibits a a trend to saturate towards higher R/L_{Ti}. For the highest value of P_{ECRH} the heat flux is higher, which is due to the additional contribution of P_{ECRH} through the energy exchange, flowing from the electron to the ion heat channel. However, more important is the steeper increase of the ion heat flux with R/L_{Ti}, revealing a clearly higher stiffness, due to the stronger destabilization of the ITG instability. Consequently the highest value of R/L_{Ti}, corresponding to on-axis NBI, is lower for this case, in agreement with the expected behaviour mentioned above that the T_i profiles remain closer to the threshold for higher stiffness.

The right plot of figure 4 illustrates the relation between ion heat flux normalized to the gyro-Bohm for the ion flux $q_{i,gB} = T_i^{2.5} n_i m_i \sqrt{2}/(e^2 B^2 R^2)$, whereby the normalization is made on the ion heat flux per unit of surface. The sets of data for each of the two ECRH powers exhibit a very clear saturation, even a decrease, towards the highest values of R/L_{Ti}. This is the impact of $T_i^{2.5}$ through the high values of T_i, see figure 3. This indicates a strong reduction of the stiffness for the on-axis NBI case, which is in agreement with the higher values of both T_i and R/L_{Ti}. This is confirmed by the gyro-kinetic calculations presented in the next sub-section and is identified to be caused by the effect of the NBI fast ions.

2.2. RESULTS FROM GYRO-KINETIC CALCULATIONS

To interpret the above results we performed linear and non-linear gyro-kinetic calculations. The former were made over a large range in turbulence wavelength which covers both ITG/TEM long wavelengths and the short wavelength region of the ETG. The non-linear calculations include electro-magnetic effects. They were carried out with the following number of modes: 43 toroidal, 339 radial et 32 along the field line. The size of the box had extensions of 80 ρ_i and 105 ρ_i in the vertical and horizontal directions respectively. They include two species or three when the NBI fast ions are taken into account. The runs were done for the two ECRH powers of 0.65 MW and 2.75 MW, at $\rho_{tor} = 0.27$ therefore for the same cases and at the same radial position as presented above for the experimental analysis.

The results and comparison with the experiment are shown in figure 5. The calculated surface integrated heat fluxes versus R/L_{Ti} are shown in the left panel. For the case with low ECRH power, we show calculations in which the effect of the NBI fast ions were included (solid symbols) or not (open symbols). If NBI ions are not taken into account Q_i and Q_e increase almost linearly with R/L_{Ti} and the heat fluxes at high R/L_{Ti} values are much larger than the experimental ones. For the calculations including NBI ions we first focus on Q_i for the case with low ECRH power, solid black circle on these plots. For the NBI off-axis case, corresponding to low R/L_{Ti}, the calculations with and without NBI ions are very similar because the NBI ion density is low (see figure 1) and the values also agree very well with the experimental ones. This also indicates that the experimental and calculated R/L_{Ti} thresholds are in good agreement. For the mixed and on-axis NBI cases the ion heat flux increases with R/L_{Ti}, which is similar to the experiment, but the values are larger than the experimental ones, in particular for the on-axis case by about a factor of two. However, they are much lower than for the cases without NBI ions,

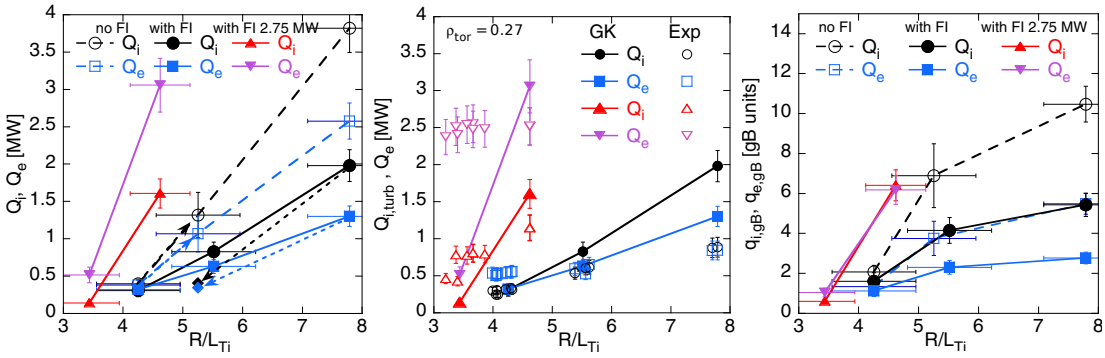

FIG. 5. Comparison of gyro-kinetic calculations and experimental results for the NBI on-axis and off-axis study. Left panel: surface-integrated heat fluxes from gyro-kinetic calculations. Middle plot: Comparison of ion heat fluxes from experiments and calculations including the NBI ions. Right panel: heat fluxes from calculations in gyro-Bohm units. The error bars on the fluxes represent the standard deviation of the calculated fluxes during the stationary state. The uncertainties on R/L_{Ti} are not indicated in the middle panel as this would confuse the plot, they are the same as in the other two plots. The various calculation cases are explained in the text. FI means NBI fast ions.

as expected from the induced stabilization. It should be pointed out that including the impact of toroidal rotation shear which is rather strong in this case has almost no effect, which we attribute to the value of ε/q which is small in this central region of the plasma. Further calculations are foreseen to assess this hypothesis.

This study is completed by two fictive variations of R/L_{Ti}. First we calculated the off-axis case, with NBI ions, for the higher value of $R/L_{Ti} = 5.2$ without changing anything else. This is indicated by the arrows upwards from left to right. This follows the cases without NBI ions, in agreement with the fact that those play almost no role for the off-axis case. This case is clearly above the mixed case with NBI ions included. The second fictive case was achieved by reducing R/L_{Ti} down to 5.2 for the on-axis case with NBI ions, as indicated by the arrows downwards from right to left. This confirms that NBI ions stabilize the ITG: the slope is somewhat flatter than without NBI ions indicating a lower stiffness, the heat flux is very low which indicates that the threshold clearly increases. We note there that a somewhat lower value of R/L_{Ti}, within the experimental uncertainty e.g. down to 7, would significantly reduce the calculated value of Q_i while the experimental values would be shifted horizontally which reduces the difference between experiment and modelling.

The case with higher ECRH power is represented by the calculations including the NBI ions for the off-axis and on-axis NBI. The ion heat flux increases strongly with R/L_{Ti} indicating a higher stiffness with higher value of T_e/T_i, as in the experiment. As shown in the middle plot, for the off-axis case the value of Q_i is very low and clearly lower than the experimental one, which could be due to the uncertainties on the R/L_{Ti} value. For the on-axis case a good agreement with the experimental values is achieved.

The ion heat flux in gyro-Bohm units shown in the right panel exhibit a clear saturation towards the highest value of R/L_{Ti}. For the electron heat flux the normalization is $q_{e,gB} = T_e T_i^{1.5} n_i m_i \sqrt{2}/(e^2 B^2 R^2)$. This is similar to the experimental case and due to the same reason: the rather high value of T_i linked to the fast ion stabilizing effect.

In summary for the ion heat flux: experiment and gyro-kinetic calculations exhibit a similar behaviour. They show that the stiffness increases with T_e/T_i and exhibit a strong stabilizing effect by NBI fast ions. The latter changes threshold and stiffness, such that, even at fixed T_e/T_i value, the points do not belong to the same threshold-stiffness curve. Consequently, the interpretation of experimental results q_i versus R/L_{Ti} generally requires support from modelling. To our knowledge, this is not specific to our experiments but valid for most of the experiments. This is also not limited to experiments with NBI as the ICRF-accelerated fast ions also play a key role, see e.g. [14, 16].

We now discuss the electron heat flux in these experiments, starting with the comparison between experiment and gyro-kinetic results in the middle panel of figure 5. For the NBI on-axis cases corresponding to the two ECRH powers, the calculated electron heat flux is comparable to the experimental one within differences which are similar to those found for the ion heat flux. This means that the high ITG turbulence in such cases is sufficient to also drive the electron heat flux, even in the presence of high ECRH power. Note that NBI ion stabilization also reduces Q_e. In contrast, for the off-axis cases, the calculated values of Q_e are much lower than the experimental ones, the difference being particularly large for the case with high ECRH power. This is due to the fact that the high electron heat flux induced by the ECRH power cannot be driven by the ITG only: as R/L_{Ti} is low the ITG is not strongly unstable. Thus, as already indicated above, an electronic instability, TEM and/or ETG, must contribute. Indeed, linear calculations over a wave length range including both ITG/TEM and ETG ranges reveal

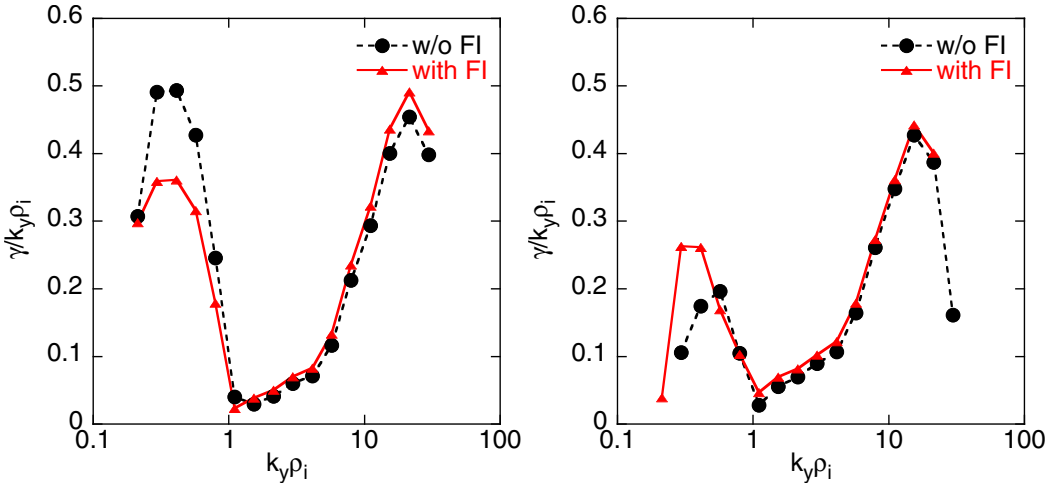

FIG. 6. Spectra from linear calculations covering the ITG-ETG wave length range. Left plot on-axis NBI case P_{ECRH} = 0.65 MW. Right plot off-axis NBI case with P_{ECRH} = 2.75 MW.

that in the off-axis case the ETG is strongly destabilized. This is illustrated in figure 6 which shows the normalized growth rates versus normalized inverse turbulence wavelength, $k_y\rho_i$, for two extreme cases: left plot on-axis NBI with 0.65 MW ECRH, right plot off-axis NBI case, for the high ECRH power of 2.75 MW. The left plot indicates a strong ITG activity and a comparable ETG activity, while in the right plot, at low R/L_{Ti} but high Q_e imposed by the ECRH power, the ETG is much stronger. The curves of the calculations with and without NBI ions indicate that linear effects stabilize the ITG at low T_e/T_i values but suggest a destabilization when T_e/T_i increases. This remains to be confirmed by additional calculations. We underline here that in this central region of the plasma, the TEM instability plays a very weak role because its threshold is quite high due to the low fraction of trapped electrons. The electron heat transport have been investigated in more details in dedicated experiments described in the next section.

3. ELECTRON HEAT CHANNEL

In the cases with significant ion heating, the ITG necessary to drive the ion heat flux might not be sufficient to drive the applied electron heat flux such that one expects TEM and/or ETG turbulence to contribute. The aim of the experiments was to search for the evidence of TEM and/or ETG driven electron heat flux above a certain level of electron heating power in addition to the NBI power. The plasmas discharges are rather similar to those performed for the study described above: same plasma current (0.8 MA) and magnetic field (2.6 T), but in this case we applied constant central NBI of 5 MW. To ensure good T_e data deduced from the modulated ECRH the ELMs were mitigated with edge magnetic perturbations which requires a density of about 7 10^{19}m^{-3}, [17]. For the investigation of the electron heat transport, we applied ECRH power deposition rather centrally ($\rho_{tor} \approx 0.3$) and more off-axis ($\rho_{tor} \approx 0.6$) varying the ratio $P_{ECRH}(0.3)/P_{ECRH}(0.6)$ while keeping the sum constant. Here also this induces a variation of the electron heat flux in the region $0.3 < \rho_{tor} < 0.6$ as well as a change of R/L_{Te} while T_e is kept almost constant at $\rho_{tor} > 0.6$ and such that the variation of T_e in the region of the analysis at $\rho_{tor} = 0.5$ is small. Applying a small modulation of the deposited ECRH power (either at $\rho_{tor} = 0.3$ or $\rho_{tor} = 0.6$) allows us to analyze the perturbative electron transport around $\rho_t = 0.5$ yielding χ_e^{HP} and compare it to χ_e^{PB}. A stronger increase of χ_e^{HP} compared to χ_e^{PB} would be a clear indication of the contribution of TEM and/or ETG to the drive of the electron heat flux. The type of turbulence can then be identified by gyro-kinetic calculations. Similar experiments were carried out in DIII-D in L-mode with rather low NBI power to study the impact of rotation by a variation of the applied NBI torque, [3].

Figure 7 left panel illustrates the increase of the electron heat flux at mid-radius as the power of ECRH deposited at $\rho_{tor} \approx 0.3$ is increased and the concomitant increase of R/L_{Te}. Note that the variations in T_e and T_i are small. The dash line represents the linear fit to the points with ECRH, excluding the one point with NBI only. It suggests a value of $R/L_{Te} \approx 6$ at the level of Q_e for NBI alone. The right panel of figure 7 reveals a strong increase of χ_e^{HP} above $R/L_{Te} \approx 7$, such that the R/L_{Te} threshold for this active instability is estimated to be close to 7. This is consistent with the threshold suggested by the heat flux in the left panel.

Similarly to the study described in the previous section, linear gyro-kinetic calculations were performed over a large range of turbulence wave-lengths which cover the ITG/TEM at low $k_y\rho_i$ and the high $k_y\rho_i$ corresponding

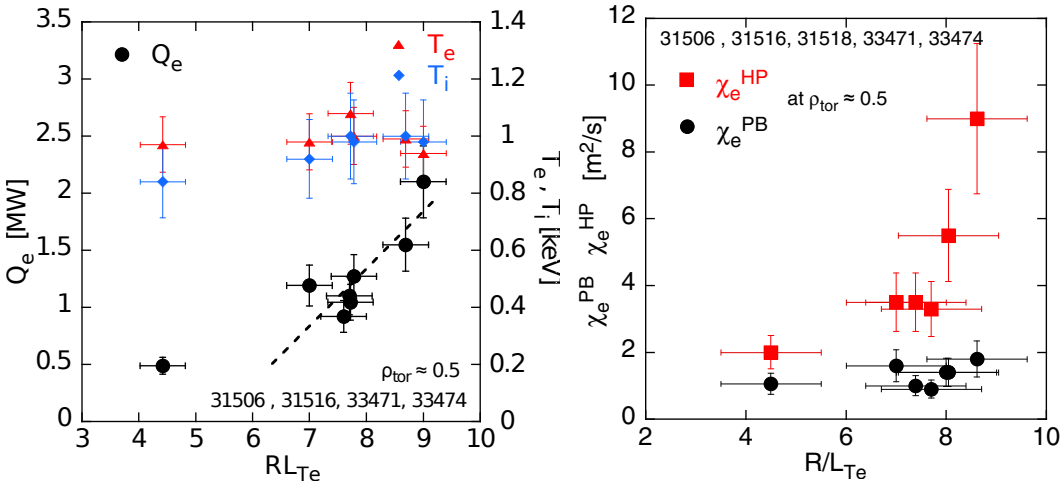

FIG. 7. Experimental values of χ_e^{PB} and χ_e^{HP} versus R/L_{Te} in the variation of the electron heat flux through ECRH, as described in the text.

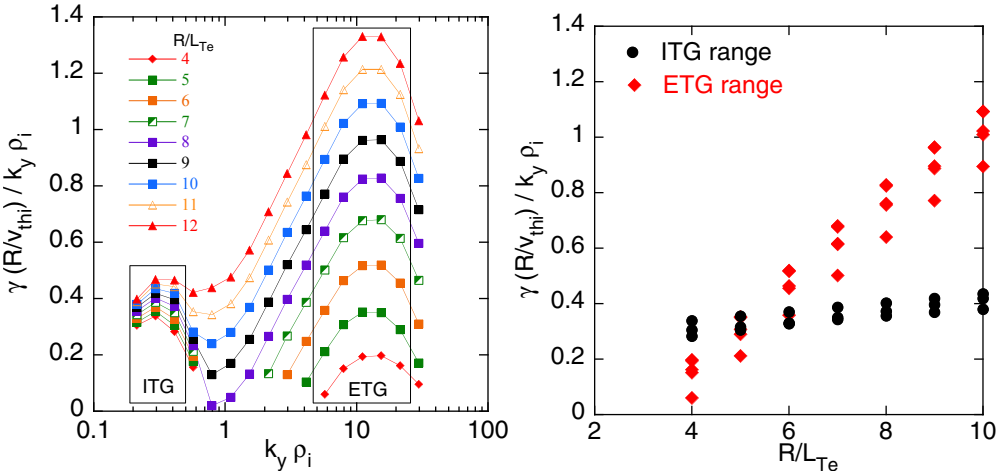

FIG. 8. Linear gyrokinetic calculations related with the increase of q_e and R/L_{Te}. Left panel contour plot of the normalized growth rate versus normalized inverse turbulence wavelength for different values of R/L_{Te}. Right panel increase of the normalized growth rate for the ITG and ETG wavelength windows indicated in the left panel.

to the ETG. The spectra are shown in figure 8 left panel: growth rates versus $k_y\rho_i$ for different values of R/L_{Te} which cover the range achieved in the experiment. They exhibit a clear increase of the growth rates for high $k_y\rho_i$ values with R/L_{Te} while the effect of R/L_{Te} is much smaller in the $k_y\rho_i$ range corresponding to ITG/TEM. The analysis of the rotation of the modes indicates that the high $k_y\rho_i$ are due to electron modes, therefore ETG, while the low $k_y\rho_i$ are strongly dominated by the ITG, a very weak contribution from TEM seems to appear as R/L_{Te} is increased. Non-linear gyro-kinetic calculations in this case should be multi-scale, which is out of the scope of this work. Selecting the ITG and ETG ranges, as indicated in figure 8 left panel and plotting the growth rates versus R/L_{Te} indicates clearly the increase of the ETG activity above $R/L_{Te} \approx 6$. This is in quantitative agreement with the increase of χ_e^{HP} shown in figure 7. In the case presented here, T_e and T_i are close to each other and it should be underlined that this situation is completely different from that obtained in low density plasmas dominated by ECRH heating with $T_e > T_i$. In such cases, the ETG threshold is very high and the TEMs dominate electron heat transport because they are strongly unstable thanks to the low collisionality and their threshold much lower than that of the ETG, [1].

The comparison of the stiffness with our previous studies on the electron heat flux and transient transport in plasmas dominated the TEM instability suggests that the ETG stiffness found here is stronger than that of the TEM.

4. DISCUSSION

The results presented here on the ITG-driven ion heat flux indicate a good agreement between theoretical calculations and experiment, although the quantitative agreement is, in some cases, only within a factor of two, the calculated values being higher than the experimental ones. The impact of T_e/T_i and NBI fast ions on the ITG stability is exhibited by the experimental analysis and confirmed by the gyro-kinetic calculations. Our study indicates clearly that the interpretation of the experimental data requires a comparison with corresponding modelling including these effects.
Results from the DIII-D tokamak, published recently in [18], indicate a clear decrease of the gyro-Bohm normalized ion heat flux with increasing R/L_{Ti} without any indication of threshold and stiffness. These experiments were based on a scan of the NBI power (2 - 8 MW) deposited centrally which induces changes of all quantities impacting on the ITG stability and gyro-Bohm normalization: T_i (including pedestal top), toroidal rotation and NBI ion content. Our study shows that indeed $q_{i,gB}$ can decrease with R/L_{Ti} but that this cannot be necessarily interpreted as an indication against the physical threshold-stiffness physics picture.
The study on electron heat transport reveals the appearance of an electron instability above a certain value of R/L_{Te} when the electron heat flux is increased with ECRH significantly above the NBI electron heat flux. This is very similar to the DIII-D results reported for L-mode at lower density and lower NBI power, [3]. While this behaviour in DIII-D is attributed to the change of the drive for the TEM from density gradient to temperature gradient, in our case the ETG is clearly the dominant contribution. It is not excluded that in the DIII-D experimental conditions the TEM threshold is lower than the ETG one, which could be compared in the frame of the ITPA joint experiment TC-13.

ACKNOWLEDGMENT

This work was partly performed within the framework of the EUROfusion Consortium and has received funding from the Euratom research and training programme 2014-2018 under grant agreement No 633053. The views and opinions expressed herein do not necessarily reflect those of the European Commission.

REFERENCES

[1] RYTER, F. et al., Nuclear Fusion **43** (2003) 1396.

[2] DEBOO, J. C. et al., Nuclear Fusion **45** (2005) 494.

[3] DEBOO, J. et al., Physics of Plasmas (2012) 082518.

[4] TUBBING, B. J. D. et al., Nucl. Fusion **27** (1987) 1843.

[5] LOPES CARDOZO, N. J. et al., Plasma Phys. Controlled Fusion **32** (1990) 983.

[6] RYTER, F. et al., Plasma Physics and Controlled Fusion **52** (2010) 124043.

[7] RYTER, F. et al., Physical Review Letters **95** (2005) 085001.

[8] PANKIN, A. et al., Computer Phys. Comm. **159** (2004) 157.

[9] ROMANELLI, F. et al., Plasma Phys. Controlled Fusion **31** (1989) 1535.

[10] GUO, S. C. et al., Physics of Fluids B: Plasma Physics **5** (1993) 520.

[11] JENKO, F. et al., Physics of Plasmas **8** (2001) 4096.

[12] WALTZ, R. E. et al., **5** (1998) 1784 .

[13] TARDINI, G. et al., Nuclear Fusion **47** (2007) 280.

[14] CITRIN, J. et al., Nuclear Fusion **54** (2014) 023008.

[15] DOERK, H. et al., Nuclear Fusion **58** (2018) 016044.

[16] SIENA, A. D. et al., Nuclear Fusion **58** (2018) 054002.

[17] SUTTROP, W. et al., Phys. Rev. Lett. **106** (2011) 225004.

[18] LUCE, T. et al., Nuclear Fusion **58** (2018) 026023.